Nuclear quantum effects on the structure and the dynamics of [H2O]8 at low temperatures

Pablo E. Videla, Peter J. Rossky, and D. Laria

Citation: J. Chem. Phys. **139**, 174315 (2013); doi: 10.1063/1.4827935
View online: http://dx.doi.org/10.1063/1.4827935
View Table of Contents: http://jcp.aip.org/resource/1/JCPSA6/v139/i17
Published by the AIP Publishing LLC.

Nuclear quantum effects on the structure and the dynamics of $[H_2O]_8$ at low temperatures

Pablo E. Videla,[1] Peter J. Rossky,[2] and D. Laria[1,3,a)]
[1]*Departamento de Química Inorgánica Analítica y Química-Física e INQUIMAE, Facultad de Ciencias Exactas y Naturales, Universidad de Buenos Aires, Ciudad Universitaria, Pabellón II, 1428 Buenos Aires, Argentina*
[2]*Department of Chemistry, The University of Texas at Austin, Austin, Texas 78712-0165, USA*
[3]*Departamento de Física de la Materia Condensada, Comisión Nacional de Energía Atómica, Avenida Libertador 8250, 1429 Buenos Aires, Argentina*

(Received 24 June 2013; accepted 18 October 2013; published online 6 November 2013)

We use ring-polymer-molecular-dynamics (RPMD) techniques and the semi-empirical q-TIP4P/F water model to investigate the relationship between hydrogen bond connectivity and the characteristics of nuclear position fluctuations, including explicit incorporation of quantum effects, for the energetically low lying isomers of the prototype cluster $[H_2O]_8$ at $T = 50$ K and at 150 K. Our results reveal that tunneling and zero-point energy effects lead to sensible increments in the magnitudes of the fluctuations of intra and intermolecular distances. The degree of proton spatial delocalization is found to map logically with the hydrogen-bond connectivity pattern of the cluster. Dangling hydrogen bonds exhibit the largest extent of spatial delocalization and participate in shorter intramolecular O-H bonds. Combined effects from quantum and polarization fluctuations on the resulting individual dipole moments are also examined. From the dynamical side, we analyze the characteristics of the infrared absorption spectrum. The incorporation of nuclear quantum fluctuations promotes red shifts and sensible broadening relative to the classical profile, bringing the simulation results in much more satisfactory agreement with direct experimental information in the mid and high frequency range of the stretching band. While RPMD predictions overestimate the peak position of the low frequency shoulder, the overall agreement with that reported using an accurate, parameterized, many-body potential is reasonable, and far superior to that one obtains by implementing a partially adiabatic centroid molecular dynamics approach. Quantum effects on the collective dynamics, as reported by instantaneous normal modes, are also discussed. [http://dx.doi.org/10.1063/1.4827935]

I. INTRODUCTION

It is well known that the light nature of protons introduces non-negligible nuclear quantum effects on the behavior of water, even at ambient conditions. This key feature can be readily perceived in the direct comparison between the thermodynamic characteristics of D_2O and H_2O. Numerous computer simulations have been conducted to trace back the microscopic origins of such differences and path-integral techniques have been demonstrated to be one of the most successful approaches to undertake such computer experiments.[1–14] The recent advent of a series of increasingly sophisticated, size-selective, spectroscopic techniques has dramatically enhanced the possibilities of gaining structural and dynamical information on aqueous systems comprised of anywhere from a handful to several hundred molecules.[15–19] The analysis of these clusters has allowed a more clear elucidation of the gradual changes that take place in passing from isolated molecule states to macroscopic bulk behaviors.[15] They have also brought forward the important role of the cluster surface and the hydrogen bonding network in understanding how water clusters interact with various other species, including polar molecules, as well as ions, including excess protons and electrons.[20–24] Since water clusters are normally generated via adiabatic expansions of aqueous vapors that bring their temperature down to the range of ∼100 K or below, one must anticipate that nuclear quantum fluctuations should manifest in a more vivid fashion.[25] Further, since the characteristic vibrational and librational frequencies of water molecules depend on their hydrogen bonding environment, it has long been appreciated that the impact of quantum effects should vary with this environment.[26] This variation should reasonably be particularly pronounced in comparing surface and more bulk-like, interior, molecules, which *a priori* have different bonding environments.

The previous considerations have provided the main motivation for the present study, in which we will present results from ring-polymer-molecular-dynamics (RPMD)[27,28] experiments to evaluate the extent of nuclear quantum effects on a series of properties pertaining to a prototype cluster, the water octamer. At sufficiently low temperatures, $[H_2O]_8$ exhibits the distinctive structural and dynamical characteristics found in bulk solids: fluctuations in the intermolecular distances much smaller than the corresponding average values and dynamical modes involving exclusively small amplitude vibrations. Several computational experiments have predicted

a)Author to whom correspondence should be addressed. Electronic mail: dhlaria@cnea.gov.ar

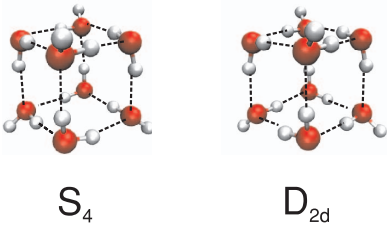

FIG. 1. $[H_2O]_8$ isomers.

that the global energy minimum configuration for the water octamer corresponds, in fact, to two, S_4 and D_{2d}, cubic- like isomers (see Fig. 1) which are practically isoenergetic.[25,29–42] The presence of these isomers has been corroborated by direct experimental evidence.[43] Considering their hydrogen bond (HB) connectivity pattern, both isomers present four water molecules acting as double-donor-single acceptors (DDSA) while the other four act as single-donor-double-acceptors (SDDA) and exhibit dangling hydrogens (H_{dng}). From a thermodynamic perspective, computer simulations have already revealed that these aggregates undergo solid-liquid phase transitions in a thermal range spanning, roughly, the 150 K–200 K interval,[31,34,44–46] and that the explicit introduction of quantum nuclear fluctuations shifts the predicted melting temperature down by about 10–20 K.[47,48]

Typically, quantum simulation studies for water have been carried out using potential energy surfaces borrowed from classical force fields for the bulk. As a possible improvement, Manolopoulos and co-workers[49] introduced the flexible q-TIP4P/F model, specifically tailored to avoid implicit quantum effects and be implemented in path-integral simulations of water. They succeeded in obtaining accurate estimates for a large variety of structural and dynamical properties of bulk liquid water. Similar lines of research have also been conducted by Voth and co-workers with their q-SPC/Fw model.[50] One might expect that such models would only provide qualitative descriptions for small clusters due to the subtleties of many-body effects in determining the potential energy surface for such systems, although for larger clusters, one would again expect to recover bulk-like behavior. Since our goals here are specifically to explore the relationship of hydrogen bonding environment and nuclear quantum fluctuations for a prototype cluster within a well defined potential basin, the use of a model such as q-TIP4P/F is completely adequate. If one were to want to quantitatively explore the fluxional regime at temperatures of 200 K and above, or that for a structurally less well defined case, such as the hexamer,[51] then a considerably more refined (and computationally more complex) potential such as the WHBB model[52] or the recently published HBB2-pol model[53,54] should be implemented. In the present case, where exploration of the cluster configurational landscape is not our goal, use of such a potential would not provide a significant benefit.

In what follows, we will analyze the combined effects from tunneling, zero-point-energy and local polarization fluctuations on the resulting interatomic spatial correlations, and charge distributions in the characteristically different water molecules forming the octamer cluster, emphasizing their particular characteristics as HB donor/acceptor. In addition, we will examine corresponding quantum effects on the overall line shape of the infrared absorption spectrum of the cluster and on the characteristics of the dynamical vibrational modes, as well.

The organization of this paper is as follows. In Sec. II, we will present details about the model and will review some basic technical details about the methodology. Information about structural characteristics and proton delocalization will be presented in Sec. III. In Sec. IV, we will discuss the dynamical implications of the incorporation of quantum effects, including a comparison among alternative methodologies. Finally, a summary of the key conclusions of the present work will be presented in Sec. V.

II. MODEL AND SIMULATION PROCEDURES

Equilibrium and dynamical properties of the water octamer were examined using the RPMD scheme developed by Manolopoulos and co-workers.[28] For time-independent averages, it is, of course, well known that the results of RPMD are equivalent to path integral (PI) statistical sampling if the simulation is thermostated or if the initial conditions for a collection of trajectories are statistically sampled in a canonical ensemble. For thermal time-independent averages, we implement the former approach and for time dependent correlations, we use the latter. We use the term RPMD throughout to describe the method used, since it correctly and compactly describes the route used here to all quantities calculated. The basic idea of this formalism relies on the consideration of the following P-bead representation of the path-integral canonical partition function for an N particle system, at a temperature T:

$$Q_P = \frac{1}{h^{3PN}} \int \cdots \int \prod_{k=1}^{P} \prod_{i=1}^{N} \mathrm{d}\mathbf{r}_i^{(k)}\, \mathrm{d}\mathbf{p}_i^{(k)} e^{-\beta_P H_P(\{\mathbf{p}_i^{(k)}\},\{\mathbf{r}_i^{(k)}\})}, \tag{1}$$

where $(P\beta_P)^{-1} = k_B T$ and

$$\begin{aligned} H_P\left(\left\{\mathbf{p}_i^{(k)}\right\},\left\{\mathbf{r}_i^{(k)}\right\}\right) &= \sum_{i=1}^{N}\sum_{k=1}^{P} \frac{\left(\mathbf{p}_i^{(k)}\right)^2}{2M_i} + U\left(\left\{\mathbf{r}_i^{(k)}\right\}\right) + V\left(\left\{\mathbf{r}_i^{(k)}\right\}\right) \\ &= \sum_{i=1}^{N}\sum_{k=1}^{P}\left[\frac{\left(\mathbf{p}_i^{(k)}\right)^2}{2M_i} + \frac{M_i\omega^2}{2}\left(\mathbf{r}_i^{(k)} - \mathbf{r}_i^{(k+1)}\right)^2\right] \\ &\quad + \sum_{k=1}^{P} V\left(\mathbf{r}_1^{(k)}, \mathbf{r}_2^{(k)}, \ldots, \mathbf{r}_N^{(k)}\right). \end{aligned} \tag{2}$$

In the previous equation, $\omega = (\beta_P\hbar)^{-1}$, whereas $\mathbf{r}_i^{(k)}$ and $\mathbf{p}_i^{(k)}$ represent the position and momentum of the ith particle of mass M_i at the imaginary time slice k, respectively ($\mathbf{r}_i^{(P+1)} = \mathbf{r}_i^{(1)}$).

As such, thermal averages for position dependent observables $\mathcal{O}(\{\mathbf{r}\})$ are expressed as statistical PI averages:[27]

$$\langle\mathcal{O}\rangle_P = \frac{1}{Q_P\, h^{3PN}} \times \int \cdots \int \prod_{k=1}^{P}\prod_{i=1}^{N} \mathrm{d}\mathbf{r}_i^{(k)}\, \mathrm{d}\mathbf{p}_i^{(k)} e^{-\beta_P H_P} \mathcal{O}_P\left(\left\{\mathbf{r}_i^{P}\right\}\right), \tag{3}$$

with

$$\mathcal{O}_P(\{\mathbf{r}_i^P\}) = \frac{1}{P}\sum_{j=1}^{P}\mathcal{O}(\{\mathbf{r}_i^j\}). \tag{4}$$

Moreover, the previous expression can be naturally extended to estimate temporal correlations between different observables as

$$\langle \mathcal{A}(0)\mathcal{B}(t)\rangle_P = \frac{1}{Q_P\, h^{3PN}}\int\cdots\int\prod_{k=1}^{P}\prod_{i=1}^{N} \mathrm{d}\mathbf{r}_i^{(k)}\,\mathrm{d}\mathbf{p}_i^{(k)}\; e^{-\beta_P H_P} \times \mathcal{A}_P(\{\mathbf{r}_i^P(0)\})\mathcal{B}_P(\{\mathbf{r}_i^P(t)\}), \tag{5}$$

where the time evolution of the set of coordinates $\{\mathbf{r}_i^P(t)\}$ is dictated by the classical equations of motion derived from the Hamiltonian appearing in Eq. (2), at a temperature $(k_B\beta_P)^{-1}$. In the present case, the potential energy term in Eq. (2) included inter and intramolecular contributions that were taken from the q-TIP4P/F flexible model.[49]

The trajectories were generated by implementing a transformation from Cartesian to normal-mode coordinates,[55] coupled to a multiple time step algorithm[56] that discriminates fast — i.e., harmonic intramolecular interactions in the polymers and intramolecular contributions to V — from the rest of the slowly varying components of the forces. Note that the normal-mode description allows for an analytical integration of Newton's equations of motions derived from the intrapolymer harmonic terms. The thermal interval covered in this study spanned from $T = 50$ K up to $T \sim 150$ K. In all cases, no evaporation episodes were registered. The number of beads was set to $P = 100$. We checked that, with this value of P, averages obtained from statistically independent experiments performed at $T = 50$ K presented, at most, 2% differences.

Two different *ad hoc* procedures were implemented to run simulation experiments: We started by considering initial S_4 configurations corresponding to an $N_w = 8$ aqueous cluster (see Fig. 1). A few test runs were also performed on the D_{2d} clusters (Fig. 1), although for all practical purposes, we found no meaningful differences between thermally averaged results from each isomer. At $T = 50$ K, no spontaneous interconversions between these two isomers were observed. To evaluate time independent properties, we run canonical trajectories lasting typically 20 ns, in which each component of each normal mode coordinate was coupled to a chain of three Nosé-Hoover thermostats,[57] set at appropriate temperatures. In doing so, we could obtain temperature control within 0.1 K. On the other hand, time dependent properties were evaluated from averages collected along one hundred different microcanonical trajectories, lasting typically ∼100 ps. The initial configurations of these microcanonical runs were taken from a set of configurations, chosen from the previous canonical run, with initial velocities generated from appropriate Boltzmann distributions.[58] In all cases, we also computed the corresponding, $P = 1$, classical trajectories.

III. SPATIAL CORRELATIONS

The starting point of our structural analysis will be the consideration of some relevant site-site spatial correlations.

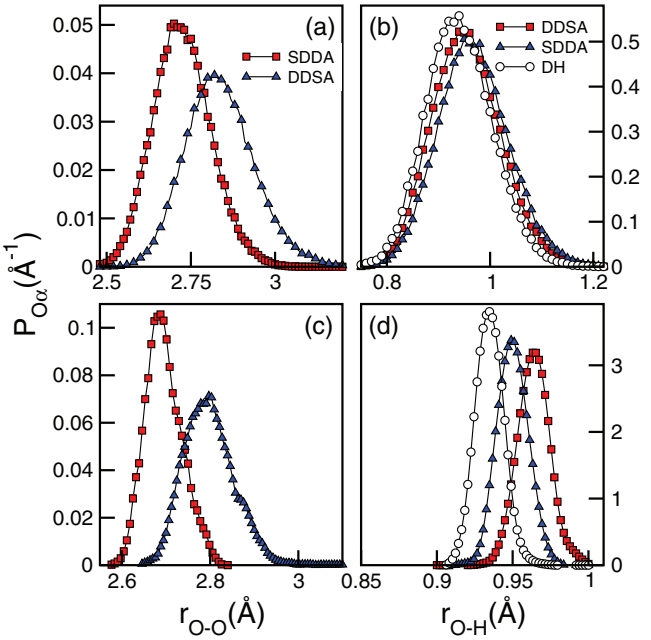

FIG. 2. Intermolecular (left panels) and intramolecular (right panels) pair correlation functions for $[H_2O]_8$ at $T = 50$ K. Top panels: RPMD results; bottom panels: classical results. The symbol labeling in the panels (c) and (d) is the same as the ones appearing in panels (a) and (b), respectively.

The four panels of Fig. 2 contain results for distributions of inter and intramolecular distances, namely:

$$P_{o\alpha}(r) = \frac{1}{P}\sum_{k=1}^{P}\left[\frac{1}{4\pi r^2}\langle\delta(r_{o\alpha}^{(k)} - r)\rangle\right], \tag{6}$$

where

$$r_{o\alpha}^{(k)} = |\mathbf{r}_o^{(k)} - \mathbf{r}_\alpha^{(k)}|. \tag{7}$$

For intermolecular distances, we focused attention on O-O distances along the twelve edges of the octamer, discriminating the eight ones in which DDSA molecules act as HB-donors from the remaining four, in which the donor waters are SDDAs. The plots in panel (a) and the analysis of the average values listed in column 2 of Table I reveal that the edges of the octamer are slightly dissimilar, with those along HBs in which DDSA water molecules act as donors being ∼0.1 Å longer than the rest. These differences have been previously reported[41] and have been ascribed to the fact that DDSA molecules would be subject to tighter constraints, imposed by the preservation of the linearity of two HBs; this fact, in turn, would also weaken their thermodynamic stabilities. We also remark that the values listed in Table I agree reasonably well with previous estimates for these distances obtained from quantum electronic calculations for minimum energy structures of the water octamer and similar small cyclic clusters.[30]

Within this context, the analysis of intramolecular O-H distances is also instructive. For these cases, we distinguished two categories: (i) $r_{OH_{dng}}$, i.e., intramolecular O-H distances involving dangling hydrogens and (ii) $r_{O-H_{con}}$, intramolecular O-H distances involving connecting hydrogens. The curves in panel (b) and the entries in columns 3 and 4 of Table I show

TABLE I. Structural parameters for $[H_2O]_8$.

H	$\langle r_{OO}\rangle$	$\langle r_{OH_{con}}\rangle$	$\langle r_{OH_{dng}}\rangle$	$\mathcal{R}_{con}$	$\mathcal{R}_{dng}$	$\langle\mu\rangle$
a. RPMD results						
SDDA	2.73	0.978	0.950	0.34	0.47	2.314
DDSA	2.84	0.964		0.36		2.334
Bulk	2.75[a]	0.978[a]				2.348[a]
b. Classical results						
SDDA	2.63	0.964	0.935			2.281
DDSA	2.70	0.950				2.302
Bulk		0.963[a]				2.311[a]

[a]From Ref. 49: Lengths are given in Angstroms, and dipole moments are expressed in Debye.

that SDDA molecules exhibit both the shortest and the longest intramolecular O-H distances. The latter characteristic could be reasonably anticipated, based on the stronger character of the HBs which, in turn, would stretch the intramolecular O-H distance in the tagged donor molecule. As a reference, also note that O-H distances in the bulk (also listed in Table I) are practically identical to those reported for $r_{OH_{con}}$ in SDDA molecules.

Effects from nuclear quantum fluctuations upon spatial correlations can gauged in a more vividly fashion by examining the profiles that appear in the bottom panels, where we present classical results (panels (c) and (d)). In all cases, the incorporation of quantum fluctuations stretches O-O distances by 0.1–0.2 Å (see entries in Table I); these changes are much less pronounced for O-H distances, where the modifications involve only $\sim 0.02 - 0.04$ Å shifts towards larger distances. Much more evident modifications are observed in the widths of the quantum distributions which, for all three $P_{OH}(r)$ cases, look $\sim$5 times wider than the classical ones.

The previous observations can be complemented with the analysis of the characteristics of the proton spatial delocalization, expressed in terms of $\mathcal{R}_i(k)$, the imaginary time mean square displacement functions of the type,[59]

$$\mathcal{R}_i^2(k) = \frac{1}{P}\sum_{j=1}^{P}\left\langle\left|\mathbf{r}_{H_i}^{(j+k)} - \mathbf{r}_{H_i}^{(j)}\right|^2\right\rangle; \quad 0 \le k \le P. \tag{8}$$

In the previous expression, $\mathbf{r}_{H_i}$ represents the coordinate of a tagged H-site ($i = con, dng$). The maximum magnitude of $\mathcal{R}_i^2$ measures the extent of quantum dispersion of particle i. Plots for $\mathcal{R}_i^2(k)$ are depicted in the top panel of Fig. 3. As a reference point, we have also included results for the free, i.e., noninteracting, proton-polymer, namely,[59]

$$\mathcal{R}_{free}^2(k) = \left(3\lambda^2\right)\ \frac{k}{P}\left(1 - \frac{k}{P}\right), \tag{9}$$

where $\lambda = 0.98$ Å represents the proton thermal wavelength at $T = 50$ K.

Results for H_{con} contrast with the ones for H_{dng} and reveal a much larger extent of spatial localization in the former category. Note that both plots for H_{con} quickly attain plateau-like characteristics along the $0.2 \lesssim k/P \lesssim 0.8$ interval, a signature that is usually ascribed to ground state dominance, that is, a thermal distribution dominated by the ground quantum state alone.[59] As such, combined effects of intra and intermolecular interactions bring the resulting sizes of the isomorphic polymers — expressed in terms of the correlation lengths $\mathcal{R}_i = \mathcal{R}_i(k/P = 0.5)$ — down to $\mathcal{R}_{con} = 0.34$ and 0.36 Å ($\sim 0.41\ \mathcal{R}_{free}$), for SDDA and DDSA molecules, respectively. On the other hand, the intra-polymer spatial correlations for H_{dng} are characterized by a larger variety of length-scales, with the longest one slightly above one half of the reference free value: $\mathcal{R}_{dng} = 0.47$ Å.

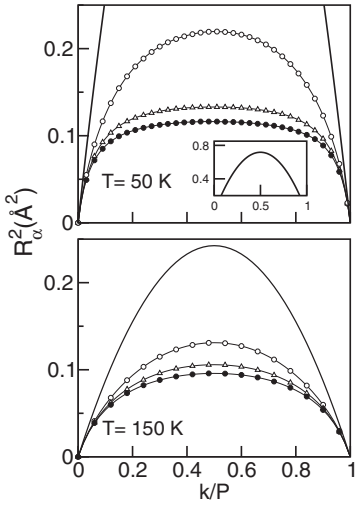

FIG. 3. Imaginary time mean square displacements for the different hydrogens in $[H_2O]_8$ at $T = 50$ K (top panel) and $T = 150$ K (lower panel). Dangling hydrogens: open circles; connecting hydrogens in DDSA waters: triangles; connecting hydrogens in SDDA molecules: black circles. Also shown are results for the thermalized, free proton-polymer: solid lines.

At this point, we briefly digress on the characteristics of a similar analysis performed in the octamer at a temperature closer to the onset of the solid-liquid transition.[31,34,44,45] Plots for $\mathcal{R}_i^2(k)$ at $T = 150$ K appear in the bottom panel of Fig. 3. Note that while the previous qualitative trends are preserved, the signatures of ground state dominance in the connecting hydrogens is much less evident and the differences between the characteristic lengthscales describing dangling and connecting protons do not surpass $\sim$0.05 Å. For H_{dng}, the shrinkage of the proton-polymer size is of the order of $\sim$25% whereas, for connecting hydrogens, the latter thermal quantum effects appear to be counterbalanced by a lesser extent of localization induced by thermal disruption of structure and a corresponding weaker intermolecular Coulomb coupling. As such, this combination results in a somewhat milder, $\sim$10% effective contraction at the higher temperature.

The average pair structure also provides information about deviations from the spherical-like structure of the proton-polymer. Assuming an ellipsoidal geometry, such deviations can be readily expressed in terms of a simple order parameter based on eccentricities ϵ_i defined in terms of

$$\epsilon_i = \left(1 - \frac{\mathcal{R}_{i,\parallel}^2}{\mathcal{R}_{i,\perp}^2}\right)^{1/2}. \tag{10}$$

In the previous equation,

$$\mathcal{R}_{i,\parallel}^2 = \frac{1}{P}\left\langle\sum_{k=1}^{P}\left[\frac{\left(\mathbf{r}_{H_i}^{(k+\frac{P}{2})} - \mathbf{r}_{H_i}^{(k)}\right)\cdot\left(\mathbf{r}_O^c - \mathbf{r}_{H_i}^c\right)}{\left|\mathbf{r}_O^c - \mathbf{r}_{H_i}^c\right|}\right]^2\right\rangle, \tag{11}$$

$$\mathbf{r}_\alpha^c = \frac{1}{P}\sum_{k=1}^{P}\mathbf{r}_\alpha^{(k)}, \tag{12}$$

and

$$\mathcal{R}_{i,\perp}^2 = \frac{1}{2}\left[\mathcal{R}_i^2 - \mathcal{R}_{i,\parallel}^2\right]. \tag{13}$$

Note that ϵ_i is close to 0 for nearly spherical hydrogen-polymers whereas it tends to 1 for prolate-like geometries along parallel and perpendicular directions with respect to the intramolecular O-H bond. Our results show that the overall polymer shapes are far from spherical: for connecting hydrogens, the combined effects between the local characteristics of intra- and intermolecular interactions are translated into eccentricities of similar magnitude: $\epsilon_{\rm con} = 0.55$ (0.57) for DDSA (SDDA) molecules. On the other hand, the local anisotropy of the confining potential acting on dangling hydrogens is much more marked, leading to eccentricities ∼20% larger, i.e., $\epsilon_{dng} = 0.67$.

To conclude this section, we consider a simple measure that captures the effects from the complex interplay between local polarization and quantum fluctuations on the charge distributions of each water molecule. We computed the corresponding magnitude of the individual molecular dipole moments. RPMD and classical results for $\langle\mu\rangle$ are listed in the last column of Table I. Two features are worth noting: (i) compared to the classical results, our simulations predict ∼1% quantum increment in all dipole moments; (ii) regardless of the particular treatment, local polarization fluctuations are somewhat more marked in DDSA molecules than in SDDA ones. The larger distortion of the overall charge distribution in the former molecules would just be a direct consequence of their participation as donors in two HBs. Yet, from a quantitative perspective, note that the magnitude of the polarization fluctuations prevailing in the octamer remain smaller than those reported in bulk water at ambient conditions, where the reported RPMD dipole moment was found to be $\langle\mu\rangle_{\rm bulk} = 2.348$ D.[49]

IV. TIME DEPENDENT RESULTS

Our dynamical analysis will focus on the characteristics of the IR absorption spectrum of the water octamer at low temperatures. The quantity of interest is the product of the spectral density $\alpha(\omega)$ times the frequency-dependent refractive index $n(\omega)$. Within the RPMD approximation, the intensity of the IR spectrum is proportional to the Fourier transform of $C_{\rm RPMD}(t)$, namely,[49,55]

$$n(\omega)\alpha(\omega) \propto \hat{C}_{\rm RPMD}(\omega) = \int_{-\infty}^{\infty} C_{\rm RPMD}(t)e^{-i\omega t}\,{\rm d}t. \tag{14}$$

In Eq. (14),

$$C_{\rm RPMD}(t) = \langle\dot{\boldsymbol{\mu}}(t)\cdot\dot{\boldsymbol{\mu}}(0)\rangle \tag{15}$$

and

$$\dot{\boldsymbol{\mu}}(t) = \frac{1}{P}\sum_{k=1}^{P}\left[\sum_{j=1}^{3N_w} z_j e\,\mathbf{v}_j^{(k)}(t)\right]. \tag{16}$$

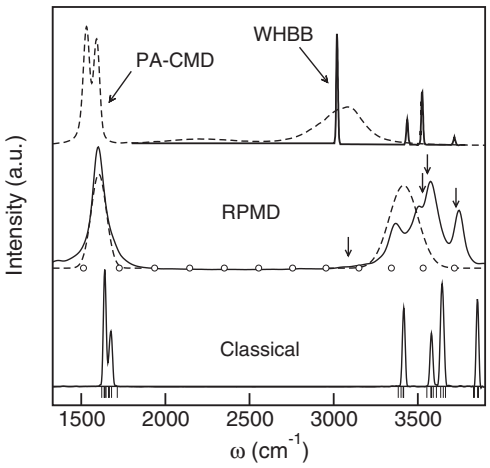

FIG. 4. RPMD (central solid line), PA-CMD (upper dashed-line), and classical (lower solid line) absorption spectra for $[H_2O]_8$ at $T = 50$ K. Also shown are the RPMD spectrum for bulk water at ambient conditions (central dashed line) taken from Ref. 49 and WHBB results for $[H_2O]_8$ (upper solid-line) taken from Ref. 69. The arrows indicate the positions of the experimental peaks taken from Ref. 43. The vertical lines at the lower part of the figure correspond to the frequencies obtained from a classical INM analysis of a quenched structure. The open circles indicate the normal mode frequencies of a free proton-polymer.

In Eq. (16), the sum over the index j involves $3N_w$ sites, with partial charges $z_j e$ and velocities $\mathbf{v}_j^{(k)}$ evaluated at the kth imaginary time slice.

In Fig. 4, we present RPMD results for the spectral intensity of $[H_2O]_8$ at $T = 50$ K, restricted to the frequency domain involving intramolecular modes. The overall lineshape can be pictured in terms of (i) a bending band at $\omega \sim 1600$ cm^{-1} and (ii) stretching band, spanning the ∼3400–3700 cm^{-1} interval. Note that, as such, the intensity profile shows no evident signs of "contaminating signals" from spurious frequencies originating from intra-polymer modes;[60] as a guide to the eye, these polymer frequencies are shown as open circles in the figure. We have verified that our methodology does manifest the substantial inaccuracies for the water monomer that have been reported elsewhere,[60] so that the present system clearly is much better behaved.

Compared to the classical lineshape, the RPMD spectrum exhibits red-shifts and sensible broadenings in both bands. At a first glance, these effects look much more prominent in the four-peak structure of the O-H stretching band although, in fact, the quantum bending band also appears structureless. It is worth noting here that the implementation of a partially adiabatic centroid molecular dynamics (PA-CMD) approach,[61] according to the scheme described in Ref. 55, does yield a double-peaked bending signal; however, in this case, the stretching band looks much more broadened and centered at ∼3100 cm^{-1} (see Fig. 4).

Before discussing the analysis of the physical interpretation of these results, we digress to analyze the internal consistency of the dynamical predictions of our RPMD scheme. This kind of analysis has been performed in the past[58,62–64] so, here, we will briefly comment on its basic elements. The time correlation function $C_{\rm RPMD}(t)$ shown in Eq. (15) provides an estimate to the following Kubo-transformed correlation

function, namely,[27]

$$C_{\mathrm{RPMD}}(t) \sim K(t) = \frac{1}{\beta Q(\beta)} \int_0^\beta d\lambda \mathrm{Tr}\,[e^{-\beta\hat{H}}\hat{\boldsymbol{\mu}}e^{i\hat{H}t/\hbar}e^{-\lambda\hat{H}}\hat{\boldsymbol{\mu}}e^{-i\hat{H}t/\hbar}e^{\lambda\hat{H}}]. \quad (17)$$

Moreover, its Fourier transform is related to the imaginary-time correlation $G(\tau)$:[58,62–64]

$$G_{\dot{\mu}}(\tau) = \frac{\beta\hbar}{\pi}\int_0^\infty d\omega \frac{\omega e^{-\beta\hbar\omega/2}}{1-e^{-\beta\hbar\omega}}\hat{C}_{\mathrm{RPMD}}(\omega) \times \cosh\left(\frac{\beta\hbar\omega}{2} - \omega\tau\right), \quad (18)$$

where

$$G_{\dot{\mu}}(\tau) = \frac{\mathrm{Tr}\,[e^{-\beta\hat{H}}\hat{\boldsymbol{\mu}}e^{-\tau\hat{H}/\hbar}\hat{\boldsymbol{\mu}}e^{\tau\hat{H}/\hbar}].}{Q(\beta)} \quad (19)$$

An equivalent expression can be obtained connecting $\hat{C}_{\mathrm{RPMD}}(\omega)$ with $R^2_\mu(\tau)$, the imaginary-time mean square displacement of the total dipole:

$$R^2_\mu(\tau) = \frac{2\beta\hbar}{\pi}\int_0^\infty d\omega \frac{e^{-\beta\hbar\omega/2}}{\omega(1-e^{-\beta\hbar\omega})}\hat{C}_{\mathrm{RPMD}}(\omega) \times \left[\cosh\left(\frac{\beta\hbar\omega}{2}\right) - \cosh\left(\frac{\beta\hbar\omega}{2} - \omega\tau\right)\right], \quad (20)$$

where

$$R^2_\mu(\tau) = \langle|\hat{\boldsymbol{\mu}}(-i\tau) - \hat{\boldsymbol{\mu}}(0)|^2\rangle = \frac{2}{Q(\beta)}\mathrm{Tr}[e^{-\beta\hat{H}}(\hat{\boldsymbol{\mu}}^2 - \hat{\boldsymbol{\mu}}e^{-\tau\hat{H}}\hat{\boldsymbol{\mu}}e^{\tau\hat{H}})]. \quad (21)$$

The computation of the imaginary-time correlation function from each of these two independent routes can be performed in a straightforward fashion using the RPMD-run (see the Appendix). In Fig. 5, we present results for $R^2_\mu(\tau)$ and $G_{\dot{\mu}}(\tau)$ obtained from the RPMD sampling and from the integrals shown in the right-hand sides of Eqs. (18) and (20). As one can see, the agreement between the two sets of results is remarkably satisfactory, a fact that provides considerable support for the quality of the RPMD dynamical description for the present system.

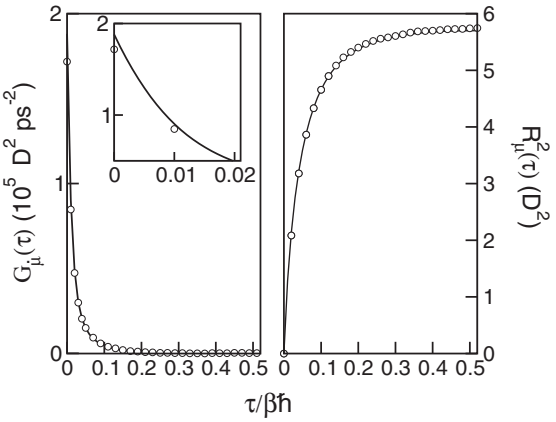

FIG. 5. Imaginary time correlation functions for the time derivative of the octamer dipole moment (left panel) and for the mean-square displacement of the total dipole moment (right panel). The solid lines correspond to integrals of the Fourier transform of the RPMD-real time correlation functions times appropriate kernels. The circles correspond to direct sampling along the RPMD runs.

An analysis of the spectrum of normal modes performed on a quenched structure of the classical S_4 isomer (also shown in Fig. 4) reveals that[43] (i) the two central peaks of the stretching band correspond to four symmetric and four asymmetric modes involving exclusively DDSA molecules, whereas the two, at the highest and the lowest energy, correspond to similar modes in SDDA molecules; (ii) in contrast, all eight bending modes exhibit much more marked, collective characteristics. A careful inspection shows that the high (low) frequency modes correspond to sets of intramolecular displacements in which groups of SDDA and DDSA molecules bend in an out-of-phase (in-phase) fashion.

Within this context, the analysis of the instantaneous normal modes[65] (INM) is also instructive. In the top panel of Fig. 6, we present results for the RPMD and classical-INM spectra, namely,

$$D(\omega) = \frac{1}{P}\sum_{k=1}^{P}\left[\sum_{i=1}^{9N_w}\langle\delta(\omega-\omega_i^{(k)})\rangle\right], \quad (22)$$

where $\omega_i^{(k)}$ represents the square root of the eigenvalues of the $9N_w \times 9N_w$ matrix:

$$V^{(k)}_{\alpha\gamma} = (M_i M_j)^{-\frac{1}{2}}\left.\frac{\partial^2 V}{\partial\alpha_i\partial\gamma_j}\right|_{\alpha_i^{(k)}\gamma_j^{(k)}}. \quad (23)$$

In Eq. (23), the Greek subindices are a shorthand notation denoting the different Cartesian coordinates of the sites.

The comparison between the classical and RPMD-INM plots shows two distinctive and interesting features: (i) an increment in the fraction of unstable frequencies from 0.07 up to 0.14 in the quantum case at the expense of the number of low-frequency, translational, and rotational modes. Based on

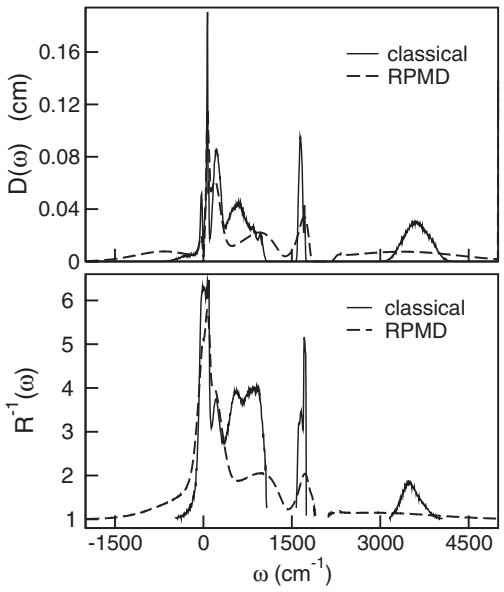

FIG. 6. Top panel: INM spectrum for $[H_2O]_8$ at $T = 50$ K. Densities for unstable modes (imaginary frequencies) appear along the negative x-axis. Bottom panel: Participation ratio spectrum for $[H_2O]_8$ at $T = 50$ K (see text).

the simple classic diffusive picture proposed by Zwanzig[66] — where the dynamics of the molecules is cast in terms of individual harmonic oscillations interrupted by jumps over saddle points that destroy the coherence of the harmonic dynamics — the increment in the number of unstable frequencies would foreshadow the lowering of the melting transition of the octamer detected in previous quantum simulations[47,48] and (ii) a sensible widening of the frequency ranges describing the different modes: Note that the original energy gap at $\omega \sim 1360\ \text{cm}^{-1}$ that, in the classical case, separates the low frequency translational and rotational bands from the bending one, is bridged by a new set of RPMD-intermediate frequencies. More dramatic are the changes affecting the range of frequencies involved in stretching motions, which now spans a much wider, $\sim$2000 cm^{-1} − 5000 cm^{-1} frequency interval.

An analysis performed on the participation ratio, $R(\omega)$, serves to quantify the extent of delocalization of the different dynamical modes, namely,[67]

$$R(\omega) = \frac{1}{D(\omega)}\left[\frac{1}{P}\sum_{k=1}^{P} R^{(k)}(\omega)\right], \tag{24}$$

where

$$R^{(k)}(\omega) = \left\langle \sum_{i}^{9N_w}\left[\sum_{j=1}^{N_w}\left(\sum_{\delta\in j}\left(e_{i,\delta}^{(k)}\right)^2\right)^2\right]\delta\left(\omega-\omega_i^{(k)}\right)\right\rangle. \tag{25}$$

In Eq. (25), the sum over the index δ includes the Cartesian coordinates of the three sites belonging to the jth molecule and $e_{i,\delta}^{(k)}$ denotes the corresponding components of the ith eigenvector of the matrix $V_{\alpha\gamma}^{(k)}$ (see Eq. (18)). The reciprocal of $R(\omega)$ is indicative of the average number of molecules contributing to different dynamical modes.

Results for $R^{-1}(\omega)$ are displayed in the bottom panel of Fig. 6. One can clearly see that RPMD modes exhibit a sensible reduction in their collective characters. Within the quantum treatment, practically all stretching modes consist of single molecule motions, whereas the bending modes, originally delocalized along two sets of SDDA and DDSA molecules, involve no more than $\sim$2 water molecules. These observation provide new evidence of the consequences of weakening interparticle Coulomb coupling, which, in turn, would simplify the description of the overall dynamics closer to a sum of uncorrelated displacements of the individual cluster components.

To conclude our presentation, we will refer to the comparison between the predicted RPMD spectrum and direct experimental information. In Fig. 4, we have included the positions of the four stretching sub-bands of the S_4 water octamer reported by Buck *et al.*[43] from infrared depletion experiments (see arrows). Clearly, the introduction of nuclear quantum fluctuations brings the classical simulation results of the three high-frequency peaks in much closer agreement with the experimental signals. In fact, for these cases, the energy differences between simulated and experimental results, barely exceed $\sim$30 cm^{-1}, at most. Contrasting, the position of the RPMD lowest frequency peak, reported by Buck *et al.* at ω = 3065 cm^{-1}, falls $\sim$200 cm^{-1} too high. This mismatch was not totally unexpected. In fact, even rather high level quantum calculations have shown similar discrepancies[30,68] which, in some cases, required *ad hoc* rescaling procedures to bring theoretical predictions in reasonable agreement with the reported experimental results.[68] Unfortunately, in our particular case, neither the normal mode analysis of the isolated molecule nor the characteristics of the bulk spectrum (also shown in Fig. 4) were able to provide clues to account for such discrepancies.

Within this context, it is also instructive to compare the present results with those recently reported by Wang and Bowman[69] for the stretching band of the water octamer, using a full-dimensional *ab initio* potential energy surface and dipole moment surface, referred to as the WHBB model (see the upper solid-curve in Fig. 4). One can observe that while the low-frequency peak at 3000–3100 cm^{-1} is much better reproduced by the WHBB model, the agreement in the high frequency stretching band regime is comparable to our RPMD predictions. As such, the quest for a model that will reproduce all the characteristics of the stretching band of the water octamer remains incomplete.

V. CONCLUDING REMARKS

The results presented in this paper provide new insights into the importance of nuclear quantum effects on structural and dynamical characteristics of the water octamer at low temperatures, and particular demonstrate the strong correlation of the characteristics of proton quantum fluctuations with hydrogen bonding environment. In a broad context, and as expected, we have verified that the explicit incorporation of such fluctuations promotes an overall weakening of hydrogen bonding in the cluster. This can be easily perceived in the 0.1–0.2 Å elongations observed in the different edges of the cubic structure, compared to the classical results. Moreover, from a quantitative perspective, the HB donor characteristics of each individual molecule control the magnitude of such modifications. Due to steric restrictions, HBs along DDSA molecules are weaker than those along SDDA ones. As a consequence, the latter molecules exhibit both the longest (along connecting hydrogens) and shortest (involving dangling H) intramolecular distances. Combined effects from the intramolecular interactions and the local characteristics of the intermolecular Coulomb coupling lead to a sensible increment in the spatial dispersion of quantized dangling hydrogens. Moreover, their "free" bonding character induces larger anisotropies in their spatial distributions. The net result of this complex interplay can be readily interpreted in terms of the small but distinct shifts in the individual dipole moments. Due to their double HB-donor role, DDSA molecules exhibit the largest polarization effects.

RPMD predictions for the positions of the mid- and high-frequency peaks of the stretching band of the IR spectrum of $[H_2O]_8$ were found to be remarkably accurate compared to experimental results. Consistency checks on the validity of the RPMD dynamics, carried out in imaginary time, support the implications that this agreement is not fortuitous. The agreement is much less satisfactory for the location of the low frequency shoulder, a fact that may be a limitation of the q-TIP4P/F model, although similar problems have been noted in other approaches.[30,68] The complementary analysis of the

INM spectrum reveals an augmentation of unstable frequencies when quantized, a fact that would sensibly open possibilities of new channels for diffusive dynamics at lower temperatures than those found in classical simulations, a result consistent with a decrease in cluster "melting point" for the quantum system. Concerning the overall characteristics of the bending and stretching modes, nuclear quantum effects also promote a sensible loss in the degree of collective character of the atomic motions, which, under these circumstances, would primarily be preserved at a molecular level.

ACKNOWLEDGMENTS

D.L. is a staff member of CONICET-Argentina. P.J.R. acknowledges the support of this research by the U.S. National Science Foundation (CHE-0910499). Additional support has been provided by the R. A. Welch Foundation (F-0019).

APPENDIX: SELF AND CROSS CONTRIBUTIONS TO $G_{\dot\mu}(\tau)$

Equations (18) and (20) establish relationships between the Fourier transform of the RPMD time correlation function for the time derivative of the total dipole of the cluster and two different imaginary time correlation functions, i.e., $R^2_\mu(\tau)$ and $G_\mu(\tau)$. Invoking the discretized P −representation of $Q(\beta)$ expressed in Eq. (1), the computation of the former quantity is fairly straightforward. Estimators for the computation of $G_{\dot\mu}(k)$ can be obtained from expressions derived in Refs. 64, 70, and 71. In particular, the evaluation of $G_{\dot\mu}(k)$ involves a sum of terms such as

$$\frac{z_i z_j}{M_i M_j}\langle \mathbf{p}_i^{(n)}\mathbf{p}_j^{(n+k)}\rangle = z_i z_j\left[\frac{3\delta_{ij}\delta_{k0}}{\beta_P M_i} - \omega_P^2\langle\left(\mathbf{r}_i^{(n)}-\mathbf{r}_i^{(n+1)}\right)\cdot\left(\mathbf{r}_j^{(n+k)}-\mathbf{r}_j^{(n+k+1)}\right)\rangle\right], \tag{A1}$$

with n arbitrary. One can resort to a generalization of the virial estimator[72] to obtain a more tractable expression of the previous equation. In particular,

$$\begin{aligned}\left\langle\left(\mathbf{r}_i^{(n)}-\bar{\mathbf{r}}_i\right)\frac{\partial V}{\partial \mathbf{r}_j^{(n+k)}}\right\rangle &\propto -\frac{1}{\beta_P}\int\cdots\int\prod_{l=1}^{3N_w}\mathrm{d}\mathbf{r}_l^{(k)}\, e^{-\beta U}\\ &\quad\times\left(\mathbf{r}_i^{(n)}-\bar{\mathbf{r}}_i\right)\frac{\partial e^{-\beta_P V}}{\partial \mathbf{r}_j^{(n+k)}}\\ &\propto \frac{1}{\beta_P}\int\cdots\int\prod_{l=1}^{3N_w}\mathrm{d}\mathbf{r}_l^{(k)}\, e^{-\beta V}\,\frac{\partial}{\partial \mathbf{r}_j^{(n+k)}}\\ &\quad\times\left[\left(\mathbf{r}_i^{(n)}-\bar{\mathbf{r}}_i\right)e^{-\beta_P U}\right]\\ &= \frac{3\delta_{ij}}{\beta_P}\left(\delta_{k0}-\frac{1}{P}\right) - M_j\omega_P^2\langle\left(\mathbf{r}_i^{(n)}-\bar{\mathbf{r}}_i\right)\\ &\quad\cdot\left(2\mathbf{r}_j^{(n+k)}-\mathbf{r}_j^{(n+k+1)}-\mathbf{r}_j^{(n+k-1)}\right)\rangle.\end{aligned} \tag{A2}$$

Combining Eqs. (A1) and (A2), the expression for the $G_{\dot\mu}(k)$ is

$$\begin{aligned}G_{\dot\mu}(k) &= \sum_{i=1}^{3N_w}\frac{z_i^2}{M_i}\left[\frac{3}{\beta}+\frac{1}{P}\sum_{n=1}^{P}\left\langle\left(\mathbf{r}_i^{(n)}-\bar{\mathbf{r}}_i\right)\frac{\partial V}{\partial \mathbf{r}_i^{(n+k)}}\right\rangle\right]\\ &\quad+\sum_{i=1}^{3N_w}\sum_{j\neq i}^{3N_w}\frac{z_i z_j}{M_j}\frac{1}{P}\sum_{n=1}^{P}\left\langle\left(\mathbf{r}_i^{(n)}-\bar{\mathbf{r}}_i\right)\frac{\partial V}{\partial \mathbf{r}_j^{(n+k)}}\right\rangle.\end{aligned} \tag{A3}$$

Considering the equivalence of all beads forming a tagged ring-polymer, the previous expression can be brought into a more symmetric one, involving a sum of self and cross correlations:

$$G_{\dot\mu}(k) = G_{\dot\mu}^{self}(k) + G_{\dot\mu}^{crss}(k), \tag{A4}$$

where

$$\begin{aligned}G_{\dot\mu}^{self}(k) &= \sum_{i=1}^{3N_w}\frac{z_i^2}{M_i}\left[\frac{3}{\beta}+\frac{1}{2P}\sum_{n=1}^{P}\left\langle\left(\mathbf{r}_i^{(n)}-\bar{\mathbf{r}}_i\right)\frac{\partial V}{\partial \mathbf{r}_i^{(n+k)}}\right\rangle\right.\\ &\quad\left.+\left\langle\left(\mathbf{r}_i^{(n+k)}-\bar{\mathbf{r}}_i\right)\frac{\partial V}{\partial \mathbf{r}_i^{(n)}}\right\rangle\right],\end{aligned} \tag{A5}$$

and

$$\begin{aligned}G_{\dot\mu}^{crss}(k) &= \sum_{i=1}^{3N_w}\sum_{j>i}^{3N_w}\frac{z_i z_j}{2P}\sum_{n=1}^{P}\frac{1}{M_j}\left[\left\langle\left(\mathbf{r}_i^{(n)}-\bar{\mathbf{r}}_i\right)\frac{\partial V}{\partial \mathbf{r}_j^{(n+k)}}\right\rangle\right.\\ &\quad\left.+\left\langle\left(\mathbf{r}_i^{(n+k)}-\bar{\mathbf{r}}_i\right)\frac{\partial V}{\partial \mathbf{r}_j^{(n)}}\right\rangle\right]\\ &\quad+\frac{1}{M_i}\left[\left\langle\left(\mathbf{r}_j^{(n)}-\bar{\mathbf{r}}_j\right)\frac{\partial V}{\partial \mathbf{r}_i^{(n+k)}}\right\rangle\right.\\ &\quad\left.+\left\langle\left(\mathbf{r}_j^{(n+k)}-\bar{\mathbf{r}}_j\right)\frac{\partial V}{\partial \mathbf{r}_i^{(n)}}\right\rangle\right].\end{aligned} \tag{A6}$$

[1] R. A. Kuharski and P. J. Rossky, J. Chem. Phys. **82**, 5164 (1985).
[2] J. Lobaugh and G. A. Voth, J. Chem. Phys. **106**, 2400 (1997).
[3] G. K. Schenter, J. Chem. Phys. **108**, 6222 (1998).
[4] L. H. de la Peña and P. G. Kusalik, J. Chem. Phys. **121**, 5992 (2004).
[5] L. H. de la Peña and P. G. Kusalik, J. Am. Chem. Soc. **127**, 5246 (2005).
[6] L. H. de la Peña, M. S. G. Razul, and P. G. Kusalik, J. Phys. Chem. A **109**, 7236 (2005).
[7] H. Gai, G. K. Schenter, and B. C. Garrett, J. Chem. Phys. **104**, 680 (1996).
[8] H. A. Stern and B. J. Berne, J. Chem. Phys. **115**, 7622 (2001).
[9] M. Shiga and W. Shinoda, J. Chem. Phys. **123**, 134502 (2005).
[10] C. D. Wick and G. K. Schenter, J. Chem. Phys. **124**, 114505 (2006).
[11] R. Ramírez and C. P. Herrero, J. Chem. Phys. **133**, 144511 (2010).
[12] G. S. Fanourgakis, G. K. Schenter, and S. S. Xantheas, J. Chem. Phys. **125**, 141102 (2006).
[13] F. Paesani, S. Iuchi, and G. A. Voth, J. Chem. Phys. **127**, 074506 (2007).
[14] T. F. Miller III and D. E. Manolopoulos, J. Chem. Phys. **123**, 154504 (2005).
[15] K. Liu, J. D. Cruzan, and R. J. Saykally, Science **271**, 929 (1996).
[16] F. N. Keutsch and R. J. Saykally, Proc. Natl. Acad. Sci. U.S.A. **98**, 10533 (2001).
[17] C. J. Gruenloh, C. A. Carney, J. R. Arrington, T. S. Zwier, S. Y. Fredericks, and K. D. Jordan, Science **276**, 1678 (1997).
[18] C. Pérez *et al.*, Science **336**, 897 (2012).
[19] U. Buck and F. Huisken, Chem. Rev. **100**, 3863 (2000).
[20] K. D. Jordan and F. Wang, Annu. Rev. Phys. Chem. **54**, 367 (2003).

[21]W. H. Robertson and M. A. Johnson, Annu. Rev. Phys. Chem. **54**, 173 (2003).
[22]J. W. Shin *et al.*, Science **304**, 1137 (2004).
[23]T. L. Guasco, B. M. Elliott, M. A. Johnson, J. Ding, and K. D. Jordan, J. Phys. Chem. Lett. **1**, 2396 (2010).
[24]R. M. Young and D. M. Neumark, Chem. Rev. **112**, 5553 (2012).
[25]B. S. González, E. G. Noya, and C. Vega, J. Phys. Chem. B **114**, 2484 (2010).
[26]D. A. Zichi and P. J. Rossky, J. Chem. Phys. **84**, 2823 (1986).
[27]I. R. Craig and D. E. Manolopoulos, J. Chem. Phys. **121**, 3368 (2004).
[28]S. Habershon, D. E. Manolopoulos, T. E. Markland, and T. F. Miller III, Annu. Rev. Phys. Chem. **64**, 387 (2013).
[29]T. Miyake and M. Aida, Chem. Phys. Lett. **427**, 215 (2006).
[30]H. M. Lee, S. B. Suh, J. Y. Lee, P. Tarakeshwar, and K. S. Kim, J. Chem. Phys. **112**, 9759 (2000).
[31]A. N. Tharrington and K. D. Jordan, J. Phys. Chem. A **107**, 7380 (2003).
[32]D. J. Wales and M. P. Hodges, Chem. Phys. Lett. **286**, 65 (1998).
[33]T. James, D. J. Wales, and J. Hernández-Rojas, Chem. Phys. Lett. **415**, 302 (2005).
[34]D. J. Wales and I. Ohmine, J. Chem. Phys. **98**, 7245 (1993).
[35]D. J. Wales and I. Ohmine, J. Chem. Phys. **98**, 7257 (1993).
[36]Q. C. Nguyen, Y. S. Ong, H. So, and J.-L. Kuo, J. Phys. Chem. A **112**, 6257 (2008).
[37]D. Laria, J. Rodriguez, C. Dellago, and D. Chandler, J. Phys. Chem. A **105**, 2646 (2001).
[38]M. Masella and F. Jean-Pierre, J. Chem. Phys. **111**, 5081 (1999).
[39]P. Nigra, M. A. Carignano, and S. Kais, J. Chem. Phys. **115**, 2621 (2001).
[40]C. J. Tsai and K. D. Jordan, J. Phys. Chem. **97**, 5208 (1993).
[41]R. Knochenmuss and S. Leutwyler, J. Chem. Phys. **96**, 5233 (1992).
[42]S. D. Belair and J. S. Francisco, Phys. Rev. A **67**, 063206 (2003).
[43]U. Buck, I. Ettischer, M. Melzer, V. Buch, and J. Sadlej, Phys. Rev. Lett. **80**, 2578 (1998).
[44]C. J. Tsai and K. D. Jordan, J. Chem. Phys. **95**, 3850 (1991).
[45]J. M. Pedulla and K. D. Jordan, Chem. Phys. **239**, 593 (1998).
[46]J. Gelman-Constantin, M. A. Carignano, I. Szleifer, E. J. Marceca, and H. R. Corti, J. Chem. Phys. **133**, 024506 (2010).
[47]E. Asare, A. R. Musah, E. Curotto, D. L. Freeman, and J. D. Doll, J. Chem. Phys. **131**, 184508 (2009).
[48]S. Shin, W.-j. Son, and S. Jang, J. Mol. Struct.: THEOCHEM **673**, 109 (2004).
[49]S. Habershon, T. E. Markland, and D. E. Manolopoulos, J. Chem. Phys. **131**, 024501 (2009).
[50]F. Paesani, W. Zhang, D. A. Case, T. E. Cheatham, and G. A. Voth, J. Chem. Phys. **125**, 184507 (2006).
[51]Y. Wang, V. Babin, J. M. Bowman, and F. Paesani, J. Am. Chem. Soc. **134**, 11116 (2012).
[52]Y. Wang, X. Huang, B. C. Shepler, B. J. Braams, and J. M. Bowman, J. Chem. Phys. **134**, 094509 (2011).
[53]V. Babin, G. R. Medders, and F. Paesani, J. Phys. Chem. Lett. **3**, 3765 (2012).
[54]G. R. Medders, V. Babin, and F. Paesani, J. Chem. Theory Comput. **9**, 1103 (2013).
[55]S. Habershon, G. S. Fanourgakis, and D. E. Manolopoulos, J. Chem. Phys. **129**, 074501 (2008).
[56]M. Tuckerman, B. J. Berne, and G. J. Martyna, J. Chem. Phys. **97**, 1990 (1992).
[57]G. J. Martyna, M. E. Tuckerman, D. J. Tobias, and M. L. Klein, Mol. Phys. **87**, 1117 (1996).
[58]A. Pérez, M. E. Tuckerman, and M. H. Müser, J. Chem. Phys. **130**, 184105 (2009).
[59]A. L. Nichols, D. Chandler, Y. Singh, and D. M. Richardson, J. Chem. Phys. **81**, 5109 (1984).
[60]A. Witt, S. D. Ivanov, M. Shiga, H. Forbert, and D. Marx, J. Chem. Phys. **130**, 194510 (2009).
[61]T. D. Hone, P. J. Rossky, and G. A. Voth, J. Chem. Phys. **124**, 154103 (2006).
[62]G. Gallicchio and B. J. Berne, J. Chem. Phys. **101**, 9909 (1994).
[63]G. Gallicchio and B. J. Berne, J. Chem. Phys. **105**, 7064 (1996).
[64]S. Habershon, B. J. Braams, and D. E. Manolopoulos, J. Chem. Phys. **127**, 174108 (2007).
[65]R. M. Stratt, Acc. Chem. Res. **28**, 201 (1995).
[66]R. Zwanzig, J. Chem. Phys. **79**, 4507 (1983).
[67]S. R. Nagel, A. Rahman, and G. S. Grest, Phys. Rev. Lett. **47**, 1665 (1981).
[68]J. Sadlej, V. Buch, J. K. Kazimirski, and U. Buck, J. Phys. Chem. A **103**, 4933 (1999).
[69]Y. Wang and J. M. Bowman, J. Phys. Chem. Lett. **4**, 1104 (2013).
[70]E. Rabani and D. R. Reichman, J. Phys. Chem. B. **105**, 6550 (2001).
[71]E. Rabani, D. R. Reichman, G. Krilov, and B. J. Berne, Proc. Natl. Acad. Sci. U.S.A. **99**, 1129 (2002).
[72]M. Herman, E. F. Bruskin, and B. J. Berne, J. Chem. Phys. **76**, 5150 (1982).